AIAA JOURNAL
Vol. 34, No. 8, August 1996

Analytical Solution for Low-Velocity Impact Response of Composite Plates

Michael O. Pierson* and Reza Vaziri†
University of British Columbia, Vancouver, British Columbia V6T 1Z4, Canada

An analytical model for the impact response of laminated composite plates is presented. The governing equations, which apply to small deflection elastic response of specially orthotropic laminates, include the combined effects of shear deformation, rotary inertia, and the nonlinear Hertzian contact law. For simply supported boundary conditions, a Fourier series solution is presented that, in contrast to previously published work, retains the frequencies associated with rotary inertia effects throughout the analysis. Errors that are incurred in the analysis of impact events, where the contact force history is obtained as part of the solution process, are investigated and guidelines to achieve converged solutions are recommended. For a benchmark impact problem, the present solution converges more rapidly than other analytical solutions available in the literature. Present analytical predictions are also found to agree well with the experimental results for composite fiber-reinforced plastic plates impacted by instrumented projectiles launched from both gas-gun and drop-weight test setups. The efficiency and robustness of the model in handling the complexities of the impact response of composite plates is further demonstrated by comparing the analytical predictions of contact force and fiber strain histories with those generated using detailed finite element analyses. The good agreement obtained instills confidence in using the model as a foundation for predictions of impact damage and response to penetrating impact events.

Introduction

LAMINATED fiber-reinforced composite plates are known to be susceptible to damage resulting from accidental impact by foreign objects. Impact on aircraft structures, for instance, from dropped tools, hail, and debris thrown up from the runway, poses a problem of great concern to designers. Since the impact response is not purely a function of material properties and depends also on the dynamic structural behavior of the composite plate, it is important to have a basic understanding of the structural response and how it is affected by different parameters. In this regard, analytical models are useful as they allow systematic parametric studies and provide a foundation for predictions of impact damage.

Although many important contributions have been made to numerical analysis of the impact response of composite plates, the corresponding analytical solutions are very few.[1] Sun and Chattopadhyay[2] used the Mindlin type shear deformation theory developed by Whitney and Pagano[3] to analyze specially orthotropic plates subjected to central impact. Dobyns[4] followed the same approach but, to avoid transverse shear force singularity at the contact point, distributed the contact force over a finite patch. Qian and Swanson[5] used a Rayleigh–Ritz procedure to obtain an approximate solution for the impact response of rectangular plates with clamped edges. Based on Laplace transform techniques, Christoforou and Swanson[6] obtained a closed-form solution by linearizing the contact force-indentation relationship. A comparison between the various solution techniques was presented by Qian and Swanson.[5] Prasad et al.[7] used a similar approach to Dobyns and modeled the impact force as a distributed patch load with cosine distribution in each direction. Noiser et al.[8] used six different models to represent the impact pressure distribution and solved the nonlinear equations of motion by a finite element scheme in time. By solving a one-parameter differential equation, Olsson[9] obtained an approximate analytical solution to the first phase of impact, or wave propagation dominated, response of composite plates.

In the present work, a robust analytical solution technique for the impact response of specially orthotropic rectangular plates is presented. Rotary inertia effects that were previously included in the formulations but ignored in the solution stage are taken into account. Present solutions for a benchmark impact problem are compared with other analytical and numerical solutions available in the literature. The predictive capability of the present analytical model is demonstrated by comparison of the results with experimental data for the impact response of composite fiber-reinforced plastic (CFRP) plates. These experimental results were obtained from impact tests involving instrumented dropped-weight (large mass, low velocity) and gas-gun propelled (small mass, high velocity) projectiles. Finally, it is shown that for a certain class of impact events where the target responds elastically, the present model produces results that are as accurate as, yet more efficient than, those generated using sophisticated finite element codes such as LS-DYNA3D.[10] The robustness of the model in handling the global structural response has proven useful in modeling penetrating impact problems where the local events due to penetration are dependent on accurate representation of the global deformations.[11]

Dynamic Response of Laminated Plates

Governing Equations

According to the first-order shear deformation theory of Whitney and Pagano,[3] the differential equations of motion for an elastic, rectangular, specially orthotropic, and symmetric laminate are given by

$$D_{11}\frac{\partial^2\psi_x}{\partial x^2}+(D_{12}+D_{66})\frac{\partial^2\psi_y}{\partial x\partial y}+D_{66}\frac{\partial^2\psi_x}{\partial y^2}-kA_{55}\left(\psi_x+\frac{\partial w}{\partial x}\right)=I\ddot{\psi}_x \tag{1a}$$

$$D_{22}\frac{\partial^2\psi_y}{\partial y^2}+(D_{12}+D_{66})\frac{\partial^2\psi_x}{\partial x\partial y}+D_{66}\frac{\partial^2\psi_y}{\partial x^2}-kA_{44}\left(\psi_y+\frac{\partial w}{\partial y}\right)=I\ddot{\psi}_y \tag{1b}$$

$$kA_{55}\left(\frac{\partial\psi_x}{\partial x}+\frac{\partial^2 w}{\partial x^2}\right)+kA_{44}\left(\frac{\partial\psi_y}{\partial y}+\frac{\partial^2 w}{\partial y^2}\right)+p_z(x,y,t)=\rho h\ddot{w} \tag{1c}$$

Received April 12, 1995; revision received Sept. 30, 1995; accepted for publication Oct. 6, 1995.

This paper is dedicated to the memory of Ernie Dost, who tragically passed away in September 1995.

*Research Engineer, Composites Group, Departments of Civil Engineering and Metals and Materials Engineering, 2324 Main Mall.

†Assistant Professor, Composites Group, Departments of Civil Engineering and Metals and Materials Engineering, 2324 Main Mall. Member AIAA.

where w is the out-of-plane displacement and ψ_x and ψ_y are the cross-sectional rotations referred to the x and y axes in the plane of the laminate, $k(=\pi^2/12)$ is a shear correction factor, ρ is the mass density of the laminate, h is the laminate thickness, $I(=\rho h^3/12)$ is the rotary inertia, and A_{ij} and D_{ij} are the usual in-plane and bending stiffness components (see, e.g., Dobyns[4]).

The homogeneous form of Eq. (1) is first solved by assuming a general harmonic solution,

$$\psi_x = e^{i\omega t} \cdot A_{mn} \cos(m\pi x/a) \sin(n\pi y/b) \tag{2a}$$

$$\psi_y = e^{i\omega t} \cdot B_{mn} \sin(m\pi x/a) \cos(n\pi y/b) \tag{2b}$$

$$w = e^{i\omega t} \cdot W_{mn} \sin(m\pi x/a) \sin(n\pi y/b) \tag{2c}$$

where A_{mn}, B_{mn}, and W_{mn} are undetermined constant coefficients, and a and b are the planar dimensions of the plate. Substituting Eq. (2) into Eq. (1) results in a set of three linear algebraic equations,

$$\begin{bmatrix} L_{11} - I\omega_{mn}^2 & L_{12} & L_{13} \\ L_{12} & L_{22} - I\omega_{mn}^2 & L_{23} \\ L_{13} & L_{23} & L_{33} - \rho h\omega_{mn}^2 \end{bmatrix} \begin{Bmatrix} A_{mn} \\ B_{mn} \\ W_{mn} \end{Bmatrix} = \begin{Bmatrix} 0 \\ 0 \\ 0 \end{Bmatrix} \tag{3}$$

where L_{ij} are the same parameters defined by Dobyns.[4]

Each solution set (m, n), results in three eigenvalues ω_{mnj} and their associated eigenvectors $[A_{mn}, B_{mn}, W_{mn}]_j$, where the subscript $j = 1, 2, 3$.

It is worth noting that in all of the previously published work, the eigenvalues associated with rotary inertia effects were ignored and thus each (m, n) pair resulted in only one eigenvalue as opposed to the three distinct eigenvalues considered here. The apparent complexity of retaining these additional frequency components in the solution was found to have very little effect on the efficiency of the analysis. Therefore, for completeness, all eigenvalues are accounted for in the present work.

To solve the particular form of Eq. (1), a separable solution is assumed, as in

$$\psi_x = \sum_{m=1}^{\infty}\sum_{n=1}^{\infty}\sum_{j=1}^{3} A_{mnj} \cdot \cos\frac{m\pi x}{a} \sin\frac{n\pi y}{b} \cdot \zeta_{mnj}(t) \tag{4a}$$

$$\psi_y = \sum_{m=1}^{\infty}\sum_{n=1}^{\infty}\sum_{j=1}^{3} B_{mnj} \cdot \sin\frac{m\pi x}{a} \cos\frac{n\pi y}{b} \cdot \zeta_{mnj}(t) \tag{4b}$$

$$w = \sum_{m=1}^{\infty}\sum_{n=1}^{\infty}\sum_{j=1}^{3} W_{mnj} \cdot \sin\frac{m\pi x}{a} \sin\frac{n\pi y}{b} \cdot \zeta_{mnj}(t) \tag{4c}$$

Substituting Eq. (4) into the equations of motion, and applying Eq. (3) yields

$$\sum_{m=1}^{\infty}\sum_{n=1}^{\infty}\sum_{j=1}^{3} A_{mnj} \cos\frac{m\pi x}{a} \sin\frac{n\pi y}{b}\left[\omega_{mnj}^2\zeta_{mnj} + \ddot{\zeta}_{mnj}\right] = 0 \tag{5a}$$

$$\sum_{m=1}^{\infty}\sum_{n=1}^{\infty}\sum_{j=1}^{3} B_{mnj} \sin\frac{m\pi x}{a} \cos\frac{n\pi y}{b}\left[\omega_{mnj}^2\zeta_{mnj} + \ddot{\zeta}_{mnj}\right] = 0 \tag{5b}$$

$$\sum_{m=1}^{\infty}\sum_{n=1}^{\infty}\sum_{j=1}^{3} W_{mnj} \sin\frac{m\pi x}{a} \sin\frac{n\pi y}{b}\left[\omega_{mnj}^2\zeta_{mnj} + \ddot{\zeta}_{mnj}\right] = \frac{p_z}{\rho h} \tag{5c}$$

To solve for the time-dependent variable ζ_{mnj}, a single equation without summation, i.e., an orthogonal set, is required. For the form of solution assumed in Eq. (4) the following orthogonality condition applies:

$$\int_0^a \int_0^b \Pi_{efg,mnj}\, dy\, dx = 0 \qquad e, f, g \neq m, n, j \tag{6}$$

where

$$\begin{aligned}\Pi_{efg,mnj} &= IA_{efg}\cos(e\pi x/a)\sin(f\pi y/b) \\ &\times A_{mnj}\cos(m\pi x/a)\sin(n\pi y/b) \\ &+ IB_{efg}\sin(e\pi x/a)\cos(f\pi y/b) \\ &\times B_{mnj}\sin(m\pi x/a)\cos(n\pi y/b) \\ &+ \rho h W_{efg}\sin(e\pi x/a)\sin(f\pi y/b) \\ &\times W_{mnj}\sin(m\pi x/a)\sin(n\pi y/b)\end{aligned} \tag{7}$$

Multiplying Eq. (5a) by $IA_{efg}\cos(e\pi x/a)\sin(f\pi y/b)$, Eq. (5b) by $IB_{efg}\sin(e\pi x/a)\cos(f\pi y/b)$, and Eq. (5c) by $\rho h W_{efg}\sin(e\pi x/a)\sin(f\pi y/b)$, then summing the three results, we obtain one equation in terms of ζ_{mnj}

$$\sum_{m=1}^{\infty}\sum_{n=1}^{\infty}\sum_{j=1}^{3}\left[\omega_{mnj}^2\Pi_{efg,mnj}\zeta_{mnj} + \Pi_{efg,mnj}\cdot\ddot{\zeta}_{mnj}\right] - \rho h W_{efg}\sin\frac{e\pi x}{a}\sin\frac{f\pi y}{b}\cdot p_z = 0 \tag{8}$$

Integrating over the laminate area meets the orthogonality condition, leaving only one nonzero term (when $e, f, g = m, n, j$), thus allowing the summation to be dropped,

$$\omega_{mnj}^2\zeta_{mnj} + \ddot{\zeta}_{mnj} = \left[\frac{(ab/4)W_{mnj}\int_0^a\int_0^b \sin(m\pi x/a)\sin(n\pi y/b)p_z\, dy\, dx}{M_{mnj}}\right] \tag{9}$$

where

$$M_{mnj} = \frac{4}{ab}\int_0^a\int_0^b \Pi_{mnj,mnj}\, dy\, dx = IA_{mnj}^2 + IB_{mnj}^2 + \rho h W_{mnj}^2 \tag{10}$$

If the eigenvectors are normalized with respect to W_{mnj} (i.e., $W_{mnj} = 1$), then the integrated term in Eq. (9) is simply the Fourier transform of the load p_z, which is assumed to be stationary, i.e.,

$$p_z = F(t)\cdot q(x, y) \tag{11}$$

The Fourier transform of the load is then

$$\int_0^a\int_0^b \sin\frac{m\pi x}{a}\sin\frac{n\pi y}{b}p_z\, dy\, dx = F(t)\cdot q_{mn} \tag{12}$$

Solving Eq. (9), using Eqs. (11) and (12), yields

$$\zeta_{mnj} = \zeta_{mnj}^0\cos(\omega_{mnj}t) + \frac{\dot{\zeta}_{mnj}^0}{\omega_{mnj}}\sin(\omega_{mnj}t) + \frac{abq_{mn}}{4\omega_{mnj}M_{mnj}}\int_0^t F(\xi)\sin\omega_{mnj}(t-\xi)\, d\xi \tag{13}$$

where the zero superscript indicates a quantity evaluated at $t = 0$.

Finally, the complete solution for lateral displacement of the laminate is

$$w = \sum_{m=1}^{\infty}\sum_{n=1}^{\infty}\sin\frac{m\pi x}{a}\sin\frac{n\pi y}{b} \times \sum_{j=1}^{3}\left\{\zeta_{mnj}^0\cos(\omega_{mnj}t) + \frac{\dot{\zeta}_{mnj}^0}{\omega_{mnj}}\sin(\omega_{mnj}t) + \frac{abq_{mn}}{\omega_{mnj}^2M_{mnj}}\int_0^t F(\xi)\sin\omega_{mnj}(t-\xi)\, d\xi\right\} \tag{14}$$

Convergence of Plate Response Solution

A closed-form convergence criterion for the Fourier solution is not available. Convergence of the solution is demonstrated numerically for a typical laminate with an applied point load and with an applied load distributed over a small patch.

The laminated plate used here as an example to examine the convergence of the plate solution is described in Table 1. This laminate, which has been considered by a number of authors (e.g., Qian and Swanson[5] and Sun and Chen[12]), will be used later as the target material for investigating the accuracy of various impact models.

For each type of loading, the central deflection of the target was calculated using 5, 10, 20, 40, 80, and 160 nonzero modes in both the x and y directions. Equation (14) was evaluated for a step load function for a range of values of t. The time integration in Eq. (14) is exact for this type of loading.

For convenience, an error estimate is calculated using the solution for 160 modes as a reference, i.e.,

$$\%\varepsilon_\chi(t) = \left|\frac{w_\chi(t)}{w_{160}(t)}\right| \cdot 100\% \qquad \chi = 5, 10, 20, 40, 80 \quad (15)$$

where

$$w_\chi = \sum_{m=1}^{(2\chi-1)} \sum_{n=1}^{(2\chi-1)} \sin\frac{m\pi}{2} \sin\frac{n\pi}{2} \times \sum_{j=1}^{3} \left\{ \zeta^0_{mnj} \cos(\omega_{mnj} t) + \frac{\dot{\zeta}^0_{mnj}}{\omega_{mnj}} \sin(\omega_{mnj} t) + \frac{abq_{mn}}{\omega^2_{mnj} M_{mnj}} \int_0^t F(\xi) \sin\omega_{mnj}(t-\xi)\, d\xi \right\} \quad (16)$$

Since even-numbered modes make no contribution to the central deflection, the nonzero mode number χ in the preceding equations corresponds to the modal indices m, n as follows:

$$m, n = 2\chi - 1 \quad (17)$$

Figures 1 and 2 plot this error function vs time. The accuracy of a modal solution is often discussed in terms of the last significant natural period of vibration as it compares to the time step. The last significant natural period for a modal solution employing χ modes is indicated in Figs. 1 and 2 by the symbol T_χ.

Table 1 Properties of the laminate used in benchmark problems to study solution accuracy

System	T300/934 CFRP plate, simply supported		
Size	200 × 200 × 2.69 mm		
Layup	$[0/90/0/90/0]_s$		
E_{11}	120 GPa	G_{12}	5.5 GPa
E_{22}	7.9 GPa	G_{13}	5.5 GPa
ν_{12}	0.33	G_{23}	5.5 GPa
h	2.69 mm	ρ	1580 kg/m^3

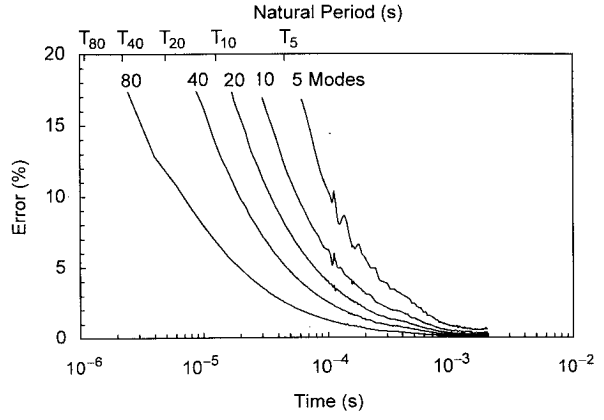

Fig. 1 Convergence of the target deflection for a step load applied at the center; 160 mode solution used as reference.

Table 2 Calculated natural frequencies for the laminate defined in Table 1

Mode no., χ	ω_{mn}, rad/s	T_χ, μs
1	1,902	3303.68
5	140,042	44.87
10	493,687	12.73
20	1,308,843	4.80
40	2,894,312	2.17
80	5,967,622	1.05
160	12,046,721	0.52

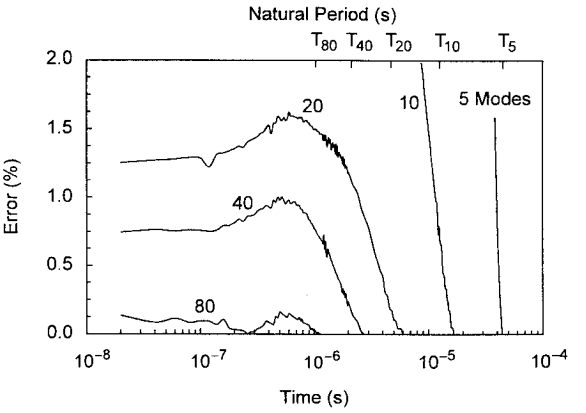

Fig. 2 Convergence of the target deflection for a step load applied over a small central patch; 160 mode solution used as reference.

For each (m, n) pair in the solution, there is a set of three natural frequencies and three modal amplitudes, as shown by Eq. (3). One frequency is associated with the lateral motion of the target, and two frequencies are attributed to the cross-sectional rotations. In general, the frequency associated with lateral motion is an order of magnitude smaller than the others. An approximate value of this dominant frequency can be calculated using [see Eq. (19) in Ref. 4]

$$\omega^2_{mn} = \left(QL_{33} + 2L_{12}L_{23}L_{13} - L_{22}L^2_{13} - L_{11}L^2_{23}\right)/(\rho h Q) \quad (18)$$

where

$$Q = L_{11}L_{22} - L^2_{12} \quad (19)$$

The (m, n)th periods are calculated using the frequencies given by Eq. (18), i.e., $T_{mn} = 2\pi/\omega_{mn}$. The natural frequencies and periods for the target described in Table 1 are listed in Table 2.

Let us define

$$\tau = h \cdot \sqrt{\rho/E_{33}} \quad (20)$$

as the time taken for a stress wave to propagate through the laminate thickness. For the target considered here $\tau = 1.2\,\mu$s. Laminate plate theory neglects the early time wave propagation behavior and considers only the gross structural response, which occurs at later times. Therefore results calculated at $t \leq \tau$ are suspect because of these stress wave effects.

Point Loading

Figure 1 shows the convergence of the laminate solution for a step load applied as a single point-force at the center of the plate. It is apparent that the number of modes required to reach reasonable accuracy is highly dependent on the time of interest.

Convergence for this type of loading is poor because of the finite shear stiffness of the target and the Fourier representation of the point force. Early in the event, the point force causes shear and flexural waves to travel outward toward the boundaries. As these waves travel outward, they act over a larger area and the wave fronts increase in circumference, resulting in reduced intensities. In the initial stages of loading, however, before these waves have time to travel, the point

load is supported by an infinitely small region of the target, resulting in infinitely large plate deformations. Thus, at times close to zero, the solution for target deflection is indeterminate. Separate convergence studies using Kirchhoff plate theory (i.e., shear deformation ignored) have shown that convergence can be obtained with a reasonable number of modes. This indicates that a modal representation of the point force is adequate and that the poor convergence is primarily because of the shear effects already described.

Convergence is obtained for times $\bar{t} > 10^{-3}$ s using a reasonably small number of modes. For solutions where $\chi > 5$, the convergence occurs at a time much greater than the last significant natural period. This type of loading is not recommended for time steps of the same order of magnitude as the normalizing parameter τ.

Patch Loading

Figure 2 shows the convergence of the laminate solution for a patch load applied at the center of the laminate. The patch area is equal to 10% of the laminate area. The jitter seen as the curves approach the time axis are because of the dynamic nature of the problem. Solutions that are slightly out of phase with the reference solution lead to deceptively large errors even after the solution has converged.

Applying the load over a patch eliminates the indeterminate problem seen in the point load solution. As expected the patch load solution converges much more rapidly than the point load solution. Each curve shown in Fig. 2 converges prior to the last significant natural period.

Typically, reasonable accuracy (0.1% error) is obtained at a time equal to the last significant natural period. The small patch solution is the most appropriate solution for impact events, as reasonable accuracy can be achieved while realistically modeling the force applied to the target.

Impact Model

To complete the formulation of the impact model we need to combine the target deformation solution with an appropriate indentation or contact law. Local indentation of the target is generally assumed to follow a Hertzian type relation. Hertz suggested that the contact between a sphere and an elastic medium could be described in terms of the total applied force F and the resulting indentation α as follows:

$$F = k_H \cdot \alpha^{\frac{3}{2}} \tag{21}$$

where k_H is the contact stiffness.

Willis[13] provided an explicit formula for k_H to describe the contact relation between a rigid sphere and a transversely isotropic half-space. Using quasistatic indentation tests on typical CFRP laminates, Tan and Sun[14] showed that the force-indentation relation can best be represented by an expression similar to Eq. (21), with k_H replaced by an experimentally determined constant k_e.

The nonlinear nature of the indentation law requires a model that is stepwise in the time domain, as in Timoshenko's incremental method.[15] Accordingly, the impact event is divided into equal segments or time steps, and the contact force is assumed to be constant through each time step. The nonlinear equations describing the impactor/target system are then solved in terms of the contact force.

At time t, the displacement of the rigid impactor Δ_p in terms of the applied force, is described by

$$\Delta_p = V \cdot t - \frac{1}{M}\int_0^t F(\xi)(t-\xi)\,d\xi \tag{22}$$

where V is the impactor velocity, and M is the impactor mass. During any time increment, Δt, in which the contact force is constant, Eq. (22) can be rewritten as

$$\Delta_p(t) = \Delta_p(t-\Delta t) + V(t-\Delta t)\cdot\Delta t - \frac{F(t)\Delta t^2}{2M} \tag{23}$$

Stepwise Form of Target Deflection

The modal solution for target deflection requires an integration over the entire history of loading. Evaluation of the target deflection is simplified by applying the transformation $\hat{t} = \Delta t$ in the time domain. The initial conditions then become

$$\zeta^0_{mnj} = \zeta_{mnj}(\hat{t}=0) = \zeta_{mnj}(t = t - \Delta t) \tag{24a}$$

$$\dot{\zeta}^0_{mnj} = \dot{\zeta}_{mnj}(\hat{t}=0) = \dot{\zeta}_{mnj}(t = t - \Delta t) \tag{24b}$$

The solution for target deflection is rewritten in a stepwise form by evaluating it at $\hat{t} = \Delta t$,

$$w = \sum_{m=1}^{\infty}\sum_{n=1}^{\infty}\sin\frac{m\pi x}{a}\sin\frac{n\pi y}{b} \times \sum_{j=1}^{3}\left\{\zeta^0_{mnj}\cos(\omega_{mnj}\Delta t) + \frac{\dot{\zeta}^0_{mnj}}{\omega_{mnj}}\sin(\omega_{mnj}\Delta t) + \frac{abq_{mn}}{\omega^2_{mnj}M_{mnj}}\int_0^{\Delta t}F(\xi)\sin\omega_{mnj}(\Delta t-\xi)\,d\xi\right\} \tag{25}$$

This stepwise form requires the initial conditions to be used at each interval and not just at $t = 0$. The initial conditions are re-evaluated at the end of each interval. This is equivalent to using initial conditions at $t = 0$ and performing the integration over the entire load history.

Equation (25) evaluated to reflect the assumption of constant contact force is

$$w = \sum_{m=1}^{\infty}\sum_{n=1}^{\infty}\sin\frac{m\pi x}{a}\sin\frac{n\pi y}{b} \times \sum_{j=1}^{3}\left\{\zeta^0_{mnj}\cos(\omega_{mnj}\Delta t) + \frac{\dot{\zeta}^0_{mnj}}{\omega_{mnj}}\sin(\omega_{mnj}\Delta t) + F(t)\frac{abq_{mn}}{\omega_{mnj}M_{mnj}}[1-\cos(\omega_{mnj}\Delta t)]\right\} \tag{26}$$

Noting that the contact force is independent of the modal summation, a simpler form of Eq. (26) can be written:

$$w = w^0(t) + C \cdot F(t) \tag{27}$$

where

$$w^0(t) = \sum_{m=1}^{\infty}\sum_{n=1}^{\infty}\sin\frac{m\pi}{2}\sin\frac{n\pi}{2} \times \sum_{j=1}^{3}\left[\zeta_{mnj}\cos(\omega_{mnj}\Delta t) + \frac{\dot{\zeta}_{mnj}}{\omega_{mnj}}\sin(\omega_{mnj}\Delta t)\right] \tag{28}$$

is the displacement because of the loading $F(t = 0 \rightarrow t - \Delta t)$, and

$$C = \sum_{m=1}^{\infty}\sum_{n=1}^{\infty}\sin\frac{m\pi}{2}\sin\frac{n\pi}{2} \times \sum_{j=1}^{3}\frac{abq_{mn}}{\omega_{mnj}M_{mnj}}[1-\cos(\omega_{mnj}\Delta t)] \tag{29}$$

is the dynamic compliance of the target.

The load is assumed, for optimum convergence, to act over a small patch equal in size to the diameter of the hemispherical projectile.

Impact Model Expressions

The form of the exponent in Eq. (21), and the linear nature of Eq. (26) allow the impact model to be formulated in closed form. Substituting the displacement expressions of Eqs. (23) and (27), into the constraint condition,

$$\Delta_p = \alpha + w \tag{30}$$

one equation in terms of a single unknown variable $F = F(t)$ is obtained

$$\lambda_0 F^3 + \lambda_1 F^2 + \lambda_2^2 F + \lambda_3^3 = 0 \tag{31}$$

where

$$\lambda_0 = -[C + (\Delta t^2/2M)]^3 \tag{32a}$$

$$\lambda_1 = -1/k_H^2 + 3\left(\Delta_p^0 - w^0 + V^0\Delta t\right)[C + (\Delta t^2/2M)]^2 \tag{32b}$$

$$\lambda_2 = \sqrt{3}\left(\Delta_p^0 - w^0 + V^0\Delta t\right)[C + (\Delta t^2/2M)]^{\frac{1}{2}} \tag{32c}$$

$$\lambda_3 = \Delta_p^0 - w^0 + V^0\Delta t \tag{32d}$$

The preceding cubic equation can be solved exactly as follows:

$$F = 2\sqrt{-\Lambda}\cos(\theta + 2n\pi) - (\lambda_1/3\lambda_0); \qquad n = 0, 1, 2 \tag{33}$$

where

$$\Lambda = \frac{3\lambda_0\lambda_2 - \lambda_1^2}{9\lambda_0^2} \tag{34}$$

$$\cos 3\theta = \frac{9\lambda_0\lambda_1\lambda_2 - 27\lambda_0^2\lambda_3 - 2\lambda_1^3}{54\lambda_0^3\sqrt{-\Lambda^3}} \tag{35}$$

In general, only one of the roots ($n = 0$) is valid.

Impact Model Convergence

Each of the displacement solutions (indentation and target deflection) are exact for a given contact force. Because the contact force history is not known a priori, however, an exact solution cannot be obtained and some error will be incurred in the solution. To investigate the convergence of the full impact model we consider the impact problem studied by Qian and Swanson.[5] This benchmark impact problem involves the impact of a 12.7-mm-diam steel ball with a mass of 8.5 g and impact velocity of 3.0 m/s against the laminate defined in Table 1. In our analysis, the contact stiffness k_H was calculated using the expression developed by Willis.[13] Convergence of the impact model is shown in Table 3 where the peak impact force is chosen as the defining characteristic and the error is defined as follows:

$$\%\varepsilon_{\Delta t}(t) = \left|\frac{\bar{F}_{\Delta t}}{\bar{F}_{0.1\,\mu s}}\right| \cdot 100\% \tag{36}$$

in which $\bar{F}_{\Delta t}$ is the peak force calculated with time step Δt, and $\Delta t = 0.1\ \mu s$ is used here as the reference solution.

Qian and Swanson[5] opted to use a 100 mode solution to calculate target deflection. The present model, however, uses a number of modes appropriate for the time step. The convergence suggested for the plate response is applied, thus the time step is chosen to be greater than the last significant natural period. Note that the natural periods listed in Table 2 are applicable here.

The different solution method applied to the present model results in different peak contact force values and an improved convergence rate. Qian and Swanson[5] used a patch of changing size corresponding to the amount of indentation. As well, they used an approximate, linear contact law as presented by Christoforou and Swanson.[6]

Table 3 Convergence of peak contact force for Qian and Swanson[5] and present impact models, as a function of time step (0.1 μs used as reference)

	Qian and Swanson[5]			Present model		
Δt, μs	No. of modes[a]	F_{max}, N	Error, %	No. of modes[a]	F_{max}, N	Error, %
10	100	179.3	37.42	5	302.2	1.10
5	100	224.8	21.54	10	300.7	0.60
2	100	255.4	10.86	15	299.5	0.22
1	100	269.7	5.86	20	299.3	0.13
0.5	100	279.4	2.48	30	299.1	0.06
0.2	100	285.3	0.42	50	298.9	0.01
0.1	100	286.5	0.00	100	298.9	0.00

[a]Indicates number of nonzero modes used in each direction.

The present model attains a reasonable level of accuracy (0.1%) with a time step of 1 μs, which corresponds to approximately 200 calculations. This is performed in a matter of seconds on a current standard personal computer (486-50 MHz).

Results and Discussion

For the impact problem considered, Figs. 3 and 4 show a comparison of the predicted time histories of the contact force and central plate deflection with published results in the literature. Qian and Swanson[5] developed a Rayleigh–Ritz solution in addition to an analytical solution based on an approximate linearized contact stiffness,[6] whereas Sun and Chen[12] used a finite element method to simulate the impact event.

Considering the approximations involved, the present model agrees quite well with the other results. Each of the previous analytical models used a changing patch size when calculating the target deflection; the present model does not. Qian and Swanson[5] used a 100 mode solution and a time step of 0.1 μs. In accordance with the convergence results, the present model used a 20 mode solution and a time step of 1 μs resulting in slightly more than 200 data points.

In an effort to assess the reliability of the present analytical model in predicting the local response, we examined the fiber strain history at the distal face (lower surface) of the laminate. Since this information was not available from the literature, we compared our analytical results with those obtained using the explicit finite element code LS-DYNA3D. Figures 5 and 6 show a comparison between the analytical and numerical predictions of the contact force and lower surface fiber strain histories for two distinctly different impact conditions. Both impact problems considered the target laminate defined in Table 1 and a spherical impactor of diam 12.7 mm. The finite element simulations were carried out using Mindlin type shell elements available in LS-DYNA3D coupled with an orthotropic elastic

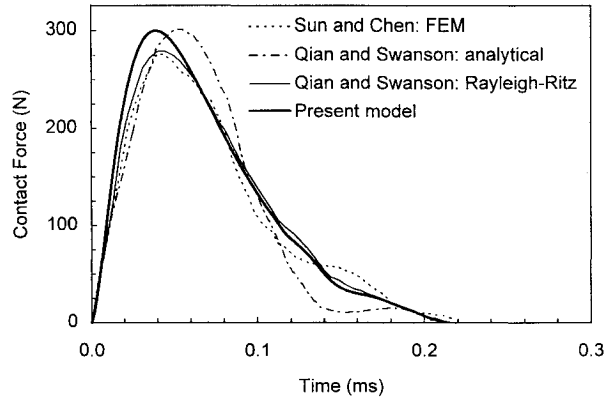

Fig. 3 Contact force history for 8.5-g, 3.0-m/s impact on the laminate defined in Table 1; present model compared with published theoretical results.[5,12]

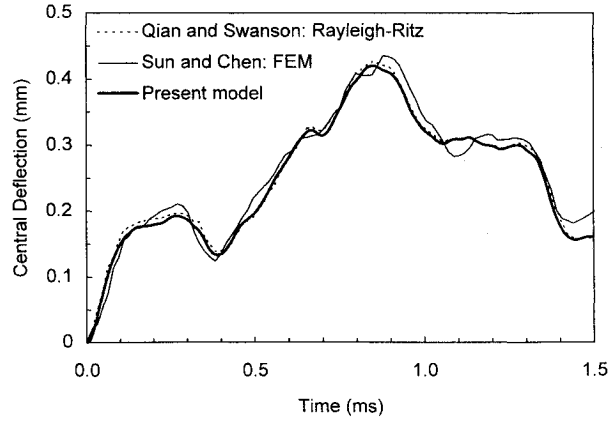

Fig. 4 Target deflection history for 8.5-g, 3.0-m/s impact on the laminate defined in Table 1; present model compared with published theoretical results.[5,12]

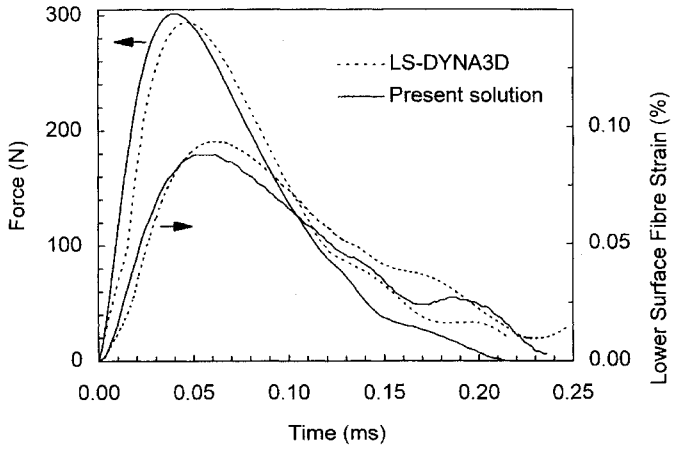

Fig. 5 Time histories of the contact force and the lower surface fiber strain at the center for 8.5-g, 3.0-m/s impact on the laminate defined in Table 1; present model compared with LS-DYNA3D results.[16]

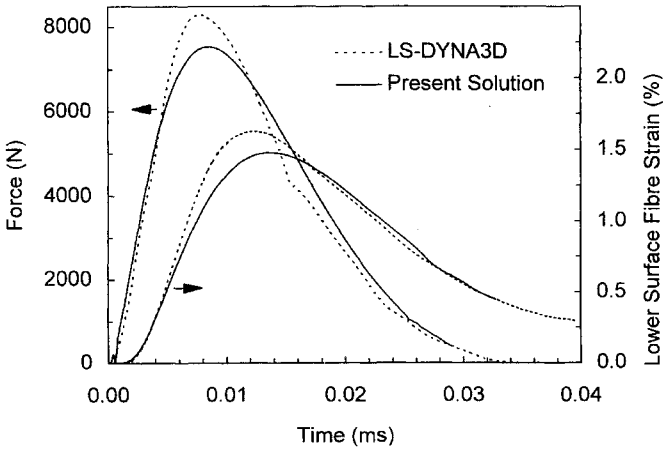

Fig. 6 Time histories of the contact force and the lower surface fiber strain at the center for 1-g, 100.0-m/s impact on the laminate defined in Table 1; present model compared with LS-DYNA3D results.[16]

representation of the laminated target. The impactor was modeled as a rigid body with its density adjusted to match the impactor mass exactly. Details of these simulations can be found in Ref. 16.

The impact event considered in Fig. 5 is identical to the benchmark problem studied before. The good agreement between the contact force histories serves as a validation of the numerical simulations. The lower surface strain histories calculated at the center of the laminate and along the fiber direction are also in good agreement. If fiber breakage at the lower surface is an indication of the onset of significant damage, as is the case for most low-velocity impact loading of thin laminates, then it can be seen that the predicted peak strains are far less than the fracture strain for carbon fibers (~1.6%). This supports our assumption of linear elastic behavior for the laminate.

To investigate the robustness and efficiency of the analytical model in handling higher velocity impact events, we considered a hypothetical impact condition involving an impactor of mass 1 g and velocity 100 m/s. Figure 6 shows a comparison between the numerical and analytical predictions for this problem. Results for the present model were obtained using a time step of 0.2 μs and 200 modes ($\chi = 200$). The close correlation between the results is encouraging considering the fact that LS-DYNA3D is a sophisticated code that is designed to handle the complexities of high-velocity impact events. Needless to say, for the same level of accuracy, the present analytical model is considerably more efficient and easier to use than the finite element analysis. It is worth pointing out that the problem is merely used to check the versatility of the analytical model, and the simulations may not represent the real behavior. At such high impact velocities, the projectile is likely to penetrate the target or cause local damage on the impact face.

Table 4 Properties of the laminate used in static indentation and impact tests

System	T800H/3900-2 CFRP plate, simply-supported		
Size	127.0 × 76.2 × 4.65 mm		
Layup	$[45/90/-45/0]_{3s}$		
E_{11}	129 GPa	G_{12}	3.5 GPa
E_{22}	7.5 GPa	G_{13}	3.5 GPa
ν_{12}	0.33	G_{23}	2.6 GPa
h	4.65 mm	ρ	1540 kg/m^3

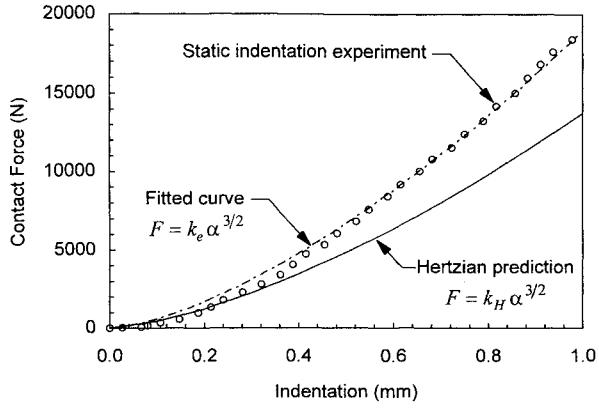

Fig. 7 Static indentation test results for the laminate defined in Table 4 compared with Hertz indentation law and with best fit curve.

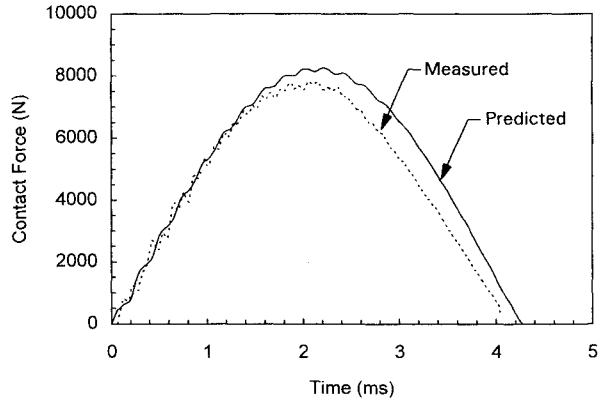

Fig. 8 Contact force history for 6150-g, 1.76-m/s impact on the laminate defined in Table 4; present model compared with drop-weight test results[18]; no target damage.

To further validate the predictive capability of the model, contact force histories collected from instrumented impact tests (see Ref. 17 for a detailed description) were used here for comparison with present results. Each impact event involved a 25.4-mm-diam hemispherically shaped projectile, and a laminated CFRP target with properties defined in Table 4. The impact tests were carried out using instrumented impactors in a drop-weight setup (corresponding to a large mass, low-velocity impact event), and a gas-gun setup (corresponding to a small mass, high-velocity impact event).[18] To establish a suitable contact law for the projectile/target system, static indentation tests were carried out. The measured force-indentation profile is shown in Fig. 7. Superposed on this curve is the response predicted by Eq. (21) with $k_H = 1.21 \times 10^9$ N/m$^{3/2}$ (calculated using the formula developed by Willis[13]), and the fitted curve obtained using $k_e = 0.60 \times 10^9$ N/m$^{3/2}$. The latter contact stiffness is used in the following impact simulations.

Figures 8–11 show the comparison between the predicted and measured contact force histories for various impact events. Note that the theoretical model, which in principle applies to specially orthotropic laminates, has been used here to analyze a quasi-isotropic laminate. However, this is not a severe restriction of the model as in this case and, indeed, in many practical cases the laminates have sufficient number of plies to render the coupling terms D_{16} and D_{26} vanishingly small.

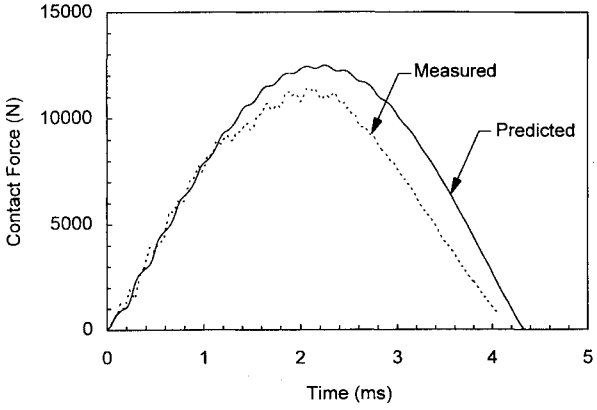

Fig. 9 Contact force history for 6150-g, 2.68-m/s impact on the laminate defined in Table 4; present model compared with drop-weight test results[18]; target damaged.

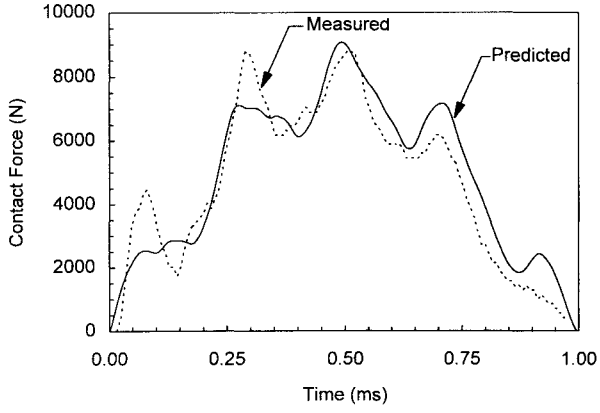

Fig. 10 Contact force history for 314-g, 7.70-m/s impact on the laminate defined in Table 4; present model compared with gas-gun test results[18]; no target damage.

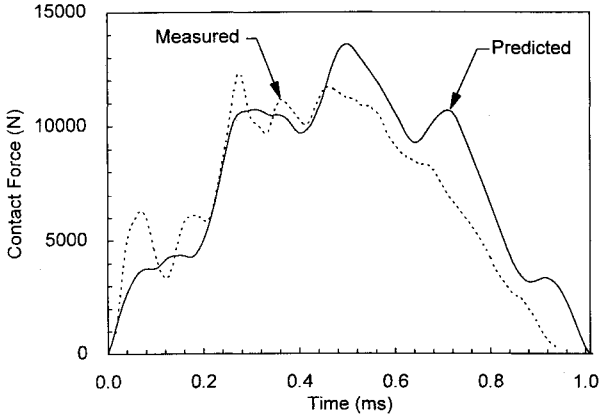

Fig. 11 Contact force history for 314-g, 11.85-m/s impact on the laminate defined in Table 4; present model compared with gas-gun test results[18]; target damaged.

For each simulation in Figs. 8–11 a suitable time step was chosen to provide sufficient detail in the resulting contact force history. In each case at least 200 points were generated by the model, with the low mass impact events requiring slightly more points to model the sharp peaks. The number of modes used to calculate target deflection was determined according to Table 5, ensuring that the last significant natural period is not greater than the time step. Note that for this laminate $\tau = 2.07\ \mu s$.

Figure 8 compares the results for a 1.76-m/s, 6.14-kg impact event (impact energy of ~9 J). The simulation used a time step of 20 μs and a five-mode solution ($\chi = 5$, and $T_\chi = 12.45\ \mu s$) for the target deflection. The analysis agrees closely with the experimental results

Table 5 Calculated natural frequencies for the laminate defined in Table 4

Mode no., χ	ω_{mn}, rad/s	T_χ, μs
1	18,122	346.71
5	504,501	12.45
10	1,115,277	5.63
20	2,314,650	2.71
40	4,701,106	1.34
80	9,467,846	0.66
160	18,998,271	0.33

in most aspects of the contact force history. The rate of loading and unloading, as well as the peak force, are accurately predicted. The analysis captures the multiple small oscillations superimposed on the measured force-time curve. These oscillations, which represent the plate vibrations, are characteristic of large-mass, low-velocity impact events where the contact duration is sufficiently long for flexural waves to reach the plate boundaries and reflect back several times. Postimpact examination of the target indicated that the target incurred no permanent damage, thus supporting the applicability of the present linear elastic analysis. Note that in the actual impact tests a portion of the incident energy (~1 J) is always dissipated and, therefore, a truly elastic response cannot be realized.

Figure 9 compares the results for a 2.68-m/s, 6.14-kg impact event (impact energy of ~22 J). Again, the simulation used a time step of 20 μs and a five-mode solution, for the target deflection. The analysis agrees closely with the experimental result in the early stages of impact. At a contact force of 8500 N the predicted response is much stiffer than that measured by the instrumented projectile. Subsequent examination of the target indicated that some damage, in the form of delaminations, had occurred during impact. The present impact model assumes a perfectly undamaged target, and thus will overestimate the stiffness if softening of the target material occurs because of damage.

Figure 10 compares the results for a 7.70-m/s, 0.314-kg impact event (impact energy of ~9 J). The simulation was performed with a time step of 5 μs and a 20-mode solution ($\chi = 20$, and $T_\chi = 2.71\ \mu s$) for the target deflection. This impact event generated a contact force history characterized by a few large-amplitude oscillations. These oscillations are the result of limited flexural wave reflections during the relatively short impact duration. Again, the analysis was capable of capturing the essence of the response quite accurately. The target did not incur permanent damage because of the impact.

Figure 11 compares the results for a 11.85-m/s, 0.314-kg impact event (impact energy of ~22 J). The simulation used a time step of 5 μs and a 20-mode solution for the target deflection. As in Fig. 9, the analysis agrees closely with the experimental results early in the impact event. At times greater than 0.4 ms, the predicted response does not agree with the experiment. This target experienced damage during impact and thus the lack of correlation is not surprising.

Based on the results described, the model is not able to predict the dynamic local response of the target in the early stages of the low-mass impact events. The measured responses shown in Figs. 10 and 11 show a peak in the contact force at a time less than 0.1 ms that is not reflected in the model predictions. Early in the impact event, the response is dominated by local indentation, as the target has not had sufficient time to deflect. The amount of indentation increases rapidly in this phase, likely giving rise to large inertial forces. However, the Hertzian relation used in the model to describe local indentation does not include any dynamic effects.

It appears that damage initiates when the contact force exceeds a critical value. For impact events where damage has occurred, the measured results deviate noticeably from the model predictions after the contact force exceeds 10,000 N (see Figs. 9 and 11). Note that for impact events not leading to damage (Figs. 8 and 10), the contact force is always less than 10,000 N.

Conclusions

An efficient analytical model for predicting the low-velocity impact response of simply supported laminated composite plates is

presented. The analysis, based on a modal solution technique, accounts for the combined effects of shear deformation, rotary inertia, and the nonlinear Hertzian contact law. All frequency components, including those associated with the rotary inertia effects, are retained throughout the solution process.

In solving the incremental equations of motion, the impact force is obtained explicitly from solution of a cubic equation, and its magnitude is assumed to remain constant during a given time step. Errors incurred in the solution, because of the coupling between the impact force and the plate displacement, have been investigated, and guidelines to achieve converged solutions are presented. It has been shown that for optimum convergence, the impact has to be modeled as a patch load and that the time step, required for the time integration of the equations, has to be greater than the last significant natural period of the plate. The model uses an appropriate number of modes for a given time step. The effectiveness and rapid convergence of the present model has been demonstrated by the successful comparison of the results with previously published analytical and numerical results for a commonly studied impact problem.

For low- and even high-velocity impact events, the present model produces results that are as accurate as, yet more efficient than, those generated using sophisticated finite element codes such as LS-DYNA3D. These results consisted of contact force-time histories as well as time histories of axial strain on the distal surface of the laminate in the fiber direction.

The predictive capability of the model has been demonstrated by comparison of the results with measured force-time curves for laminated CFRP plates subjected to drop-weight and gas-gun impact events. Results suggest that the model is able to predict the essential features of the contact force history in both these cases up until the onset of damage in the laminate. Beyond this point, the linear elastic assumption of the model is no longer valid and the contact force is overpredicted.

The analytical model presented here is useful for design purposes where efficient analysis tools are required for systematic parametric studies. Furthermore, the robustness of the model in handling the transient structural response of composite plates provides a reliable foundation for predictions of impact damage and response to penetrating impact events.

Acknowledgments

Financial support for this work was provided by the Canadian Department of National Defence under a contract with the Directorate Research and Development Land (contract monitor: René Larose), and the Natural Science and Engineering Research Council of Canada through a research grant to the second author. The authors would like to thank Kevin Williams for carrying out the numerical computations using LS-DYNA3D. Thanks are also extended to Anoush Poursartip, Daniel Delfosse, and Roger Bennett of the Composites Group at the University of British Columbia; Ernie Dost of the Boeing Commercial Airplane Company, Seattle, Washington; and Brian Coxon of Integrated Technologies, Bothell, Washington, for providing the experimental results.

References

[1]Abrate, S., "Impact on Laminated Composite Materials," *Applied Mechanics Review*, Vol. 44, No. 4, 1991, pp. 155–190.

[2]Sun, C. T., and Chattopadhyay, S., "Dynamic Response of Anisotropic Laminated Plates Under Initial Stress to Impact of a Mass," *Journal of Applied Mechanics*, Vol. 42, Sept. 1975, pp. 693–698.

[3]Whitney, J. M., and Pagano, N. J., "Shear Deformation in Heterogeneous Anisotropic Plates," *Journal of Applied Mechanics*, Vol. 37, Dec. 1970, pp. 1031–1036.

[4]Dobyns, A. L., "Analysis of Simply-Supported Orthotropic Plates Subject to Static and Dynamic Loads," *AIAA Journal*, Vol. 19, No. 5, 1981, pp. 642–650.

[5]Qian, Y., and Swanson, S. R., "A Comparison of Solution Techniques for Impact Response of Composite Plates," *Composite Structures*, Vol. 14, No. 3, 1990, pp. 177–192.

[6]Christoforou, A. P., and Swanson, S. R., "Analysis of Impact Response in Composite Plates," *International Journals of Solids and Structures*, Vol. 27, No. 2, 1991, pp. 161–170.

[7]Prasad, C. B., Ambur, D. R., and Starnes, J. H., Jr., "Response of Laminated Composite Plates to Low-Speed Impact by Different Impactors," *AIAA Journal*, Vol. 32, No. 6, 1994, pp. 1270–1277.

[8]Noiser, A., Kapania, R. K., and Reddy, J. N., "Low-Velocity Impact of Laminated Composites Using a Layerwise Theory," *Computational Mechanics*, Vol. 13, No. 5, 1994, pp. 360–379.

[9]Olsson, R., "Impact Response of Orthotropic Composite Plates Predicted from a One-Parameter Differential Equation," *AIAA Journal*, Vol. 30, No. 6, 1992, pp. 1587–1596.

[10]Hallquist, J. O., "LS-DYNA3D—Nonlinear Dynamic Analysis of Structures in Three Dimensions," LS-DYNA3D User's Manual, Livermore Software Technology Corp., Livermore, CA, 1990.

[11]Pierson, M. O., "Modelling the Impact Behaviour of Fibre Reinforced Composite Materials," M.S. Thesis, Dept. of Metals and Materials Engineering, Univ. of British Columbia, Vancouver, BC, Canada, Sept. 1994.

[12]Sun, C. T., and Chen, J. K., "On the Impact of Initially Stressed Composite Laminates," *Journal of Composite Materials*, Vol. 19, 1985, pp. 490–504.

[13]Willis, J. R., "Hertzian Contact of Anisotropic Bodies," *Journal of Mechanics and Physics of Solids*, Vol. 14, 1966, pp. 163–176.

[14]Tan, T. M., and Sun, C. T., "Use of Statical Indentation Laws in the Impact Analysis of Laminated Composite Plates," *Journal of Applied Mechanics*, Vol. 52, 1985, pp. 6–12.

[15]Timoshenko, S. P., "Zur Frage nach der Wirkung eines Stosses auf einen Balken," *Zeitschrift für Mathematik und Physik*, Vol. 62, No. 2, 1913, p. 198.

[16]Williams, K. V., and Vaziri, R., "Finite Element Analysis of the Impact Response of CFRP Composite Plates," *Proceedings of the 10th International Conference on Composite Materials (ICCM-10)* (Whistler, BC, Canada), Woodhead Publishing, Cambridge, England, UK, 1995, pp. V-647–V-654.

[17]Delfosse, D., Pageau, G., Bennett, R., and Poursartip, A., "Instrumented Impact Testing at High Velocities," *Journal of Composites Technology and Research*, Vol. 15, No. 1, 1993, pp. 38–45.

[18]Delfosse, D., Vaziri, R., Pierson, M. O., and Poursartip, A., "Analysis of the Non-Penetrating Impact Behaviour of CFRP Laminates," *Proceedings of the 9th International Conference on Composite Materials* (Madrid, Spain), Vol. 5, Woodhead Publishing, Cambridge, England, UK, 1993, pp. 366–373.